
Brichau, Stephanie; Ring, Uwe; Ketcham, Richard A.; Carter, Andrew; Stockli, Daniel and Brunel, Maurice (2006). Constraining the long-term evolution of the slip rate for a major extensional fault system in the central Aegean, Greece, using thermochronology. *Earth and Planetary Science Letters* 241 (1-2) 293-306.

Constraining the long-term evolution of the slip rate for a major extensional fault system in the central Aegean, Greece, using thermochronology

Stephanie Brichau

Department of Geology, University of Kansas, Lawrence KS 66045, USA

Uwe Ring

Department of Geological Sciences, University of Canterbury, Christchurch 8004, New Zealand

Andrew Carter

School of Earth Sciences, University and Birkbeck College, London WC1E6BT, UK

Richard A. Ketcham

Jackson School of Geosciences, University of Texas, Austin, TX 78712, USA

Daniel Stockli

Department of Geology, University of Kansas, Lawrence KS 66045, USA

Maurice Brunel

UMR 5573, Université Montpellier II, 34095 Montpellier Cedex 05, France

Correspondence to: Stéphanie Brichau, email: brichau@ku.edu, phone: +1-785-864-7657, fax: +1-785-864-7789

Abstract: The brittle/ductile transition is a major rheologic boundary in the crust yet little is known about how or if rates of tectonic processes are influenced by this boundary. In this study we examine the slip history of the large-scale Naxos/Paros extensional fault system (NPEFS), Cyclades, Greece, by comparing published slip rates for the ductile crust with new thermochronologic constraints on slip rates in the brittle regime. Based on apatite and zircon fission track (AFT and ZFT) and (U-Th)/He dating we recognize an increase in the slip rate across the brittle/ductile transition on Naxos. ZFT and AFT ages range from 11.8±0.8 to 9.7±0.8 Ma and 11.2±1.6 to 8.2±1.2 Ma and (U-Th)/He zircon and apatite ages are between 10.4±0.4 to 9.2±0.3 Ma and 10.7±1.0 to 8.9±0.6 Ma, respectively. On Paros, ZFT and AFT ages range from 13.1±1.4 Ma to 11.1±1.0 Ma and 12.7±2.8 Ma to 10.5±2.0 Ma while the (U-Th)/He zircon ages are slightly younger between 8.3±0.4 Ma and 9.8±0.3 Ma. All ages consistently decrease northwards in the direction of hangingwall transport. Published slip rates of ~5-6 km Myr^{-1} constrain the speed of the NPEFS in the ductile regime between 16-12 Ma on Naxos. When integrated with our new data it seems that the slip rate increased from ~5-6 km Myr^{-1} to ~8-9 km Myr^{-1} across the brittle/ductile transition. Based on published modeling work we propose that the brittle/ductile transition is a main storage of elastic energy and a local heat source. Localization of shear in the semi-brittle regime is thought to be document by widespread formation of frictional melts (pseudotachylites), the latter of which formed when fault slip accelerated on Naxos. The data also show that the NPEFS accomplished a minimum total offset of ~50 km between ~16-8 Ma.

Key-words: Aegean Sea, extensional faulting, slip rate, brittle/ductile transition.

Introduction

Some extensional provinces on Earth are characterized by high rates of deformation. The Basin-and-Range province of the western United States and the Aegean Sea are classic examples [1-5]. Research over the last decade has demonstrated that extensional faults can slip at rates from ~1 km Myr^{-1} up to >20 km Myr^{-1} [4-11]. In general these rates are time averaged and do not supply information as to whether the rate of tectonic processes changes systematically over time, distance and across the brittle/ductile transition, which is the major rheologic boundary in the Earth's crust.

The Aegean Sea in the eastern Mediterranean (Fig. 1) achieved >~250 km of extension since the Miocene [12] at an average rate of >~15 km Myr^{-1}. It seems likely that most of this extension took place on a few major normal fault systems [10, 13, 14]. If so, the slip rates on

each of these faults have to be high, >~5 km Myr^{-1}. High rates of extensional slip exceeding ~5 km Myr^{-1} have been reported from the Khelmos detachment on the Peleponnesus [8], the Cretan detachment on the island of Crete [15], the Vari detachment on Syros and Tinos islands [11], the Messaria extensional system on Ikaria Island [14] and from the Menderes extensional province in adjacent western Turkey [16, 17]. These extensional detachments largely operated in the brittle crust and originated near the brittle/ductile transition, a domain that is usually thought to be the strongest layer of the lithosphere [18]. Unravelling the speed of tectonic processes, and also how the speed of these processes varies over time, distance and across rheologic boundaries, is of primary importance if we are to understand the pervasive deformation and internal structure of wide and diffuse plate-boundary zones.

The Naxos/Paros extensional fault system (NPEFS) is an unusually complete fault system consisting of a thick lower-crustal ductile shear zone grading upwards into a thin brittle detachment [6, 19, 20] and extends laterally over more than 30 km (Fig. 2). Therefore, it presents an ideal opportunity (1) to constrain slip rates from deep-crustal to near-surface conditions across the brittle/ductile transition and (2) to constrain possible lateral changes in the timing and speed of fault slip.

Herein, we use zircon and apatite fission-track and (U-Th)/He thermochronometry for constraining the slip rate at the NPEFS in the brittle crust of Naxos and Paros. Our new data will then be compared and integrated with the slip rates for the ductile part of the crust reported in [6] to see if slip rates change across the brittle/ductile transition in Naxos. The latter aim may shed new light on this important rheologic boundary and if it has a significant influence on rates of continental extension. The data from Naxos and Paros also permit detection of whether slip rates vary systematically along strike of major extensional systems.

Setting

Previous research has shown that the Hellenides comprise a series of high-pressure belts that formed successively above the southward retreating Hellenic subduction zone. The Cycladic blueschist unit is the dominant tectonic unit in the central Aegean. It is fringed to the north by the oceanic Vardar-Izmir-Ankara suture zone, the Lycian nappes, and the Pelagonian zone (Fig. 1). The Cycladic blueschist unit comprises in descending order three composite nappe units: (1) a mélange-like unit of ophiolitic rocks underlain by (2) a post-Carboniferous shelf sequence, and (3) a Carboniferous basement unit [21]. In some windows in the Cycladic zone, metasediments of the Basal unit as part of the External Hellenides crops out below the Cycladic blueschist unit. The Cycladic blueschist unit is tectonically overlain on a number of

islands by the largely non-metamorphosed Upper unit. On Naxos and Paros, the NPEFS forms the contact between the Cycladic blueschist and Upper unit. Detailed work [20, 22, 23] demonstrated that the extensional fault systems on Naxos and Paros can be correlated with each other and form the NPEFS.

The metamorphic evolution of the Cycladic blueschist unit includes an Eocene high-pressure event commencing at ~55 Ma followed by a greenschist-facies overprint [24-27]. High-pressure metamorphism in the Basal unit on Evia and Samos islands is dated at 24-21 Ma [15]. In the Middle to Late Miocene the Cyclades became part of the magmatic arc of the southward retreating Hellenic subduction zone as evidenced by arc-related volcanic rocks ranging from ~12-5 Ma [28] and granites spanning an age range from ~15-10 Ma [29]. The present arc is located to the south of the Cyclades and mimics the southward retreat of the subduction zone.

The geology of Naxos and Paros islands is dominated by the Cycladic blueschist unit (Fig. 2). In contrast to all other Cycladic islands, the high-pressure rocks were overprinted on both islands by Miocene amphibolite-facies metamorphism that reached anatectic conditions on Naxos (670±50°C and 5-7 kbar) [30, 31]. For Paros, maximum Miocene temperatures of ~650°C were estimated [32], which suggests similar metamorphic conditions on both islands. Furthermore, on both islands the Carboniferous basement and the overlying shelf sequence depict a concentric, onion-shaped pattern of rock units and isograds [30, 32]. This pattern resembles a migmatite and mantled gneiss dome also suggesting that maximum PT conditions on Paros were not significantly lower than those on Naxos [20]. During the waning stages of high-grade metamorphism S-type granites intruded the Cycladic blueschist unit between ~15-11 Ma [29, 33]. High-temperature metamorphism and intrusion of the S-type granites was synchronous with ductile extensional deformation within the >1 km thick, shallowly dipping Naxos/Paros extensional shear zone [13], which is the ductile expression of the NPEFS. It has been convincingly argued that high-temperature metamorphism on Naxos developed as a consequence of ductile extensional shearing [19, 31]. Extensional deformation started at or before the peak of high-temperature metamorphism, which has been dated at ~20-16 Ma on Naxos [29, 33, 34].

The broad ductile shear zone of the NPEFS grades tectonically upward into the narrow (~20-30 m thick) brittle Naxos/Paros detachment, the latter of which is interpreted as the upper crustal expression of the NPEFS [6, 19, 20]. At ~12 Ma, a huge granodiorite body (>15 km diameter) intruded the western part of Naxos Island [33, 35]. This granodiorite is part of the Late Miocene magmatic arc of the southward retreating Hellenic subduction zone and

intruded synkinematically into the footwall of the brittle NPEFS exposed on Naxos [19]. Numerous pseudotachylites associated with the brittle NPEFS formed in the granodiorite [13] and one sample yielded a K/Ar age of 9.9±0.4 Ma [35]. Metasomatic fronts, cinder cones, drusy quartz fillings on pervasive crack systems, opaline quartz as well as iron and sulphur staining indicate pronounced hydrothermal activity of overpressured fluids at the brittle NPEFS exposed on Naxos [29].

The hangingwall of the NPEFS is mainly made up by the very thin and non-metamorphosed Upper unit. Kinematic indicators show a consistent top-NNE sense of shear on the NPEFS [19, 20]. Structural work shows that top-NNE extension was coeval with E-W shortening, which together controlled the shapes of the high-grade domes on Naxos and Paros.

The slip rate for the ductile shear zone of the NPEFS has been constrained on Naxos Island by [6], who showed that the K/Ar and $^{40}Ar/^{39}Ar$ ages on biotite, white mica and hornblende [33-36] become systematically younger northwards in the direction of hangingwall transport on the NPEFS. For slip-rate calculations only ages <16 Ma were used because it was argued that only those ages can be safely related to movement on the NPEFS [6]. Slip rates of 5.1 (+0.6/-0.5) km Myr^{-1} (K/Ar on biotite), 7.6 (+3.7/-1.9) km Myr^{-1} (K/Ar on white mica) and 4.7 (+3.5/-1.4) km Myr^{-1} ($^{40}Ar/^{39}Ar$ on hornblende) were estimated [6]. However, [34] showed that white mica on Naxos is a mixture of blueschist-facies phengite (>50 Ma) and muscovite belonging to the ≥16 Ma high-temperature event. Therefore, the slip rate derived from white mica is probably an artifact and will not be used herein. It is important to note that these data constrain the slip rate on the NPEFS in the ductile regime.

Sampling and Methodology

The brittle/ductile transition occurs at lowest greenschist-facies conditions [37] at the high end of the zircon fission track (ZFT) partial annealing zone (PAZ), which is placed between ~300-200°C [38]. For the apatite fission track (AFT) system the PAZ is between ~110-60°C [39]. Recent studies [40, 41] constrain the zircon Helium (He) partial retention zone (PRZ) between ~190-120°C, while in apatite He is partially retained between 80°C and 40°C (He partial retention zone, PRZ) [42]. Thus, by using a combination of zircon and apatite fission-track and (U-Th)/He thermochronometry it is possible to monitor cooling in the brittle crust between ~300°C to ~40°C. To obtain slip rates for the brittle NPEFS, we collected six samples from granitic rocks in the footwall of the NPEFS exposed on Naxos and three

samples in the gneissic basement of the Cycladic blueschist unit of Paros, along a NNE-SSW profile parallel to the tectonic transport direction of the NPEFS (Fig. 2).

Calculating the slip rate on the NPEFS on Naxos and Paros islands in the temperature range between ~300°C to ~40°C serves two purposes: (1) it allows us to constrain the evolution of the slip rate in the brittle crust and, in conjunction with the published ductile slip rates to monitor the slip rate across the brittle/ductile transition on Naxos and, (2) because sampling along NNE profiles was done some 20-25 km away from each other, it allows constraints to be placed on any lateral changes in the timing and rate of fault slip in the brittle range by comparing the fission-track and (U-Th)/He ages from Naxos and Paros islands.

Samples for fission-track analysis were irradiated at the Radiation Center of Oregon State University, USA. Fission-track ages were calibrated by the ζ method [43] and ages were calculated using the central-age method [44], which allows for extra-poissonian variation within a population of single-grain ages belonging to a single sample. Apatite and zircon (U-Th)/He age (AHe and ZHe) determinations were carried out at the California Institute of Technology and University of Kansas laboratories, respectively. Detailed laboratory procedures are described elsewhere [40, 45, 46]. Reported ages are corrected for α-ejection effects based on measured grain dimensions [47]. He and U determinations were replicated and a mean age is reported. The estimated analytical uncertainty for both apatite and zircon He ages is ~6% (2σ), in agreement with the reproducibility observed for the samples.

Slip rates were estimated by fitting a line to the age-distance data. The fitting procedure used χ^2 minimization incorporating both measured age uncertainties and an estimated uncertainty of 1 km (2σ) in distance (Tables 1 and 2). Uncertainties were estimated using a Monte Carlo procedure in which each point was varied according to its measured and estimated uncertainties using a Gaussian random-number generator, and a line was fit to each deviated set of points. Ten thousand sets of deviates were generated, and the top and bottom 2.5% of results were discarded to estimate 95% probability limits (Table 3). For the AFT data on Naxos, rates were fitted to all of the samples measured (Na1-Na6), and also to the subset for which the other thermochronometric data were obtained (Na3-Na6), to facilitate direct comparison of the derived rates. Samples Na1 and Na2, being closest to the detachment, record the final stage of unroofing.

Age data

Apatite and zircon fission track and (U-Th)/He ages are quoted to the 2σ level (Table 1 and 2). On Naxos, ZFT ages range between 11.8±0.8 Ma and 9.7±0.8 Ma and AFT ages from

11.2±1.6 Ma to 8.2±1.2 Ma. Apatite mean track lengths are between 14-15 μm. ZHe and AHe ages range from 10.4±0.4 to 9.2±0.3 and 10.7±0.5 Ma to 8.9±0.3 Ma, respectively. From Paros, fission tracks on apatite and zircon and (U-Th)/He on zircon were measured. Numerous fluid and zircon inclusions in the apatites prevented (U-Th)/He dating. Samples yield ZFT ages from 13.1±1.4 Ma to 11.1±1.0 Ma while AFT are between 12.7±2.8 Ma and 10.5±2.0 Ma. Apatite mean track lengths are 14-15 μm. ZHe ages range from 9.8±0.3 to 8.3±0.4 Ma.

Slip rates

The ages obtained from each method gave internally consistent results that systematically decrease northwards in the direction of hanging wall slip. The northward decrease in ages reflects the lateral passage of isotherms at the top of the footwall and can be used to estimate slip rates from the inverse slope of mineral ages with distance in the slip direction [5-7] (Fig. 2). The results yield slip rates (Table 3) for the brittle NPEFS exposed on Naxos of 6.4 (+6.8/-2.2) km Myr^{-1} (ZFT), 13.2 (+9.4/-4.5) km Myr^{-1} (ZHe), 8.0 (+11.8/-3.0) km Myr^{-1} (AFT) and 9.3 (+5.3/-2.6) km Myr^{-1} (AHe) (Fig. 3a), while for Paros the obtained slip rates are 6.9 (+13.7/-3.5) km Myr^{-1} (ZFT), 6.1 (+2.8/-1.6) km Myr^{-1} (zircon (U-Th)/He) and 6.1 (+2.8/-1.6) km Myr^{-1} (AFT) (Fig. 3b). The errors are relatively large but χ^2 reduced values are very small. For the FT data χ^2 reduced values range from 0.05 to 0.001 while probabilities of fit are close to one (0.892 to 0.995). This indicates that errors on slopes and therefore on slip rates are markedly overestimated. For the ZHe data from Naxos, a χ^2 reduced value of 1.054 and the probability of fit of 0.523 indicate that the slip rate estimation and associated error are realistic. Nonetheless, the AHe data from Naxos with a χ^2 reduced of 6.789 and the low probability of fit (0.005) indicate a significant mismatch, which may reflect additional unquantified errors in the data or that the linear fit is inappropriate. Possibilities for the poor fit include a non-linear slip rate or that the near-surface cooling patterns had an additional influence aside from the direct effect of fault slip.

On Naxos, the ZFT, ZHe, AFT and AHe ages from the four samples collected in the granodiorite overlap within error and together with the long apatite track-length data (>14 μm) support very rapid cooling from ~300°C to ~40°C within <2 Ma. The data yield a cooling rate of the granodiorite of ~110°C Myr^{-1} between ~12-9 Ma. On Paros, the ZHe ages are slightly younger than the AFT ages. The anomalously young ZHe ages might be explained by U and Th zoning. Zircon fission-track mounts show thin, but highly U-enriched rims. Therefore

using a traditional F_T correction assuming homogeneous U and Th distribution would lead to a substantial underestimation of the F_T correction and consequently of our ZHe ages [39, 46]. Nonetheless, the ZFT and AFT ages overlap within error and together with the long apatite track-length data (>14 μm) support very rapid cooling of the gneissic basement on Paros between ~13-10 Ma. Overall, the cooling of the Naxos granodiorite and the Paros basement seems to be similarly fast indicating a common cooling history.

Thermal modeling

To help interpret the thermochronometric data, and especially to see whether the derived slip rates were significantly influenced by advecting isotherms and the granodiorite intrusion on Naxos, finite element thermal models of tectonic unroofing of Naxos and Paros were performed using the methods described by [48]. The models all assume that the detachment dips at 30° and plunges to an arbitrary depth of 45 km before leveling off. Exhumation is accommodated entirely by lateral motion of the hanging wall and vertical motion of the footwall crust and mantle. The typical finite element dimension is 2165 m wide by 1250 m deep, and the starting model space was 121 km wide by 120 km deep. Material properties are for granite in the crust and olivine in the mantle; the upper crust (0-25 km) is given a heat production of 1 $\mu W/m^3$, and the lower crust one of 0.39 $\mu W/m^3$. The model starting condition is defined by the peak temperature of amphibolite-facies metamorphism, which we take as a temperature of approximately 680°C at a depth of 23 km corresponding approximately to the position of sample Na2. This required using a basal heat flux of 50 mW/m^2. Although this value is probably unreasonably high, and the high initial gradient is more likely due to transient processes than steady-state conditions, it does not appreciably affect our estimates of cooling patterns in the near-surface regime. Model starting times were ~16 Ma, depending on constraints imposed by slip rate and intrusion time and depth. Models were evaluated by tracing the thermal histories at a set of points representing the sample positions, and comparing both the inferred ages and slip rates to our measurements. Sample positions are assumed to lie at a uniform depth ~0.5 km below the detachment surface.

We used the models to test the hypothesis that Naxos and Paros unroofed simultaneously and at similar rates, with the only difference being the granodiorite intrusion on Naxos. We simulated Paros and the central and eastern parts of Naxos outside the aureole of the granodiorite intrusion using a slip rate of 6.5 km Myr^{-1}. For this model predictions of inferred slip rates successfully replicated all of our measured slip rates on Paros to within 1 km Myr^{-1}. Furthermore, the model also indicated that isotherm advection would cause the slip rate

inferred from the hornblende K-Ar system to be reduced to 4.2 km Myr^{-1}, close to the value observed by [6] for central and eastern Naxos. The slip rates for the low-temperature systems are not affected by isotherm advection to any significant degree.

The intrusion of the granodiorite on Naxos was approximated by instantaneously resetting the model nodes it encompasses to 700°C at 12.3 Ma; at the time of intrusion it lay largely along the trace of the dipping detachment, spanning depths from 3.8-12.5 km. Although a model with a constant slip rate of 6.5 km Myr^{-1} gave age and inferred slip rate predictions close to our AFT and ZFT results, slightly better fits to the AFT ages for samples Na1 and Na2 were achieved with a model featuring late acceleration to 8.0 km Myr^{-1}. The primary discrepancies were for the Naxos slip rates derived from the AHe and ZHe systems, for which the model-inferred values of ~6.5 km Myr^{-1} were significantly below the measured rates. For the cases simulated, the modelling demonstrated that the effect of the granodiorite intrusion on Naxos is to reduce the ages by 1-1.5 Myr and slightly increase the inferred slip rates by 0-1.5 km Myr^{-1}. Overall, the modelling exercise showed that the cooling rates and thus derived slip rates were not greatly affected by the granodiorite intrusion, as cooling was still primarily controlled by tectonic unroofing, albeit from a radically altered thermal state.

Discussion

Lateral variations of ages

The AFT and ZFT ages from Paros are on average ~1.0-1.5 Myr older than those from Naxos. This age difference, across a distance of ~20-25 km, can be accounted for in four different ways: (1) the simplest explanation would be that the Paros samples were collected from more southerly localities with respect to the NPEFS, therefore cooled earlier and yielded older ages. It has indeed been proposed [49] that the putative Mid Cyclades lineament runs through western Paros (Fig. 2) and displaced the western part of Paros, where our samples come from, dextrally with respect to eastern Paros and Naxos. Dextral offset on the Mid Cyclades lineament could account for the older ages from western Paros. The two AFT ages of 9.9±1.1 Ma and 9.3±0.6 Ma reported by [50] from southeastern Paros, i.e. east of the Mid-Cyclades lineament, are perfectly in line with this interpretation, especially since these ages are similar to our age for sample Na4, which is from a structurally comparable position on Naxos. In Figure 4a a dextral offset on the Mid Cyclades lineament has been restored. Because the AFT and ZFT ages of samples Ps3 and Na5 are very similar, we used both sample localities as a piercing point, which would results in a net dextral offset of ~10 km on the Mid-Cyclades lineament. (2) The different fission-track ages from Naxos and Paros reflect

lateral changes in the timing of slip on different segments of the NPEFS. It is a well-known feature from active faults like the North Anatolian fault, the San Andreas faults or various subduction thrusts worldwide that recent slip on those large-scale structures occurs heterogeneously, i.e. different segments of a fault slip at different times. Likewise, we suggest that slip on ancient faults also occurred heterogeneously. Previous works showed that the displacement distribution on a fault can be quite irregular [51] and that fault growth might be inhibited at the contacts of dissimilar lithologies [52]. If the latter case was true for the NPEFS, then the fault might have locked for some time when it cut though the shelf sequence of the Cycladic blueschist unit. The intrusion of the Naxos granodiorite at ~12 Ma might have unlocked the fault and aided slip through the shelf sequence on Naxos. All these complexities make it likely that slip on large-scale faults may actually occur laterally at different times (Fig. 4b). (3) It is also possible that the correlation shown in Fig. 4b holds and that the difference in ages was caused by the granodiorite intrusion rather than changes in the timing or rate of slip between the two islands. This is the scenario we tested with our modeling. Although we were able to match many of our age and rate observations well, the thermal effect of the intrusion was not in itself enough to replicate the higher slip rate inferred from the ZHe data for Naxos. (4) The correlation of the NPEFS between Naxos and Paros as proposed by several authors [20, 22, 23] is not justified and the extensional fault systems on both islands represent two different detachments that operated at different times. Given the detailed geologic and structural mapping [20, 22, 23] revealing very similar geology in the foot- and hangingwall of the NPEFS, a similar structural evolution from ductile to brittle conditions and consistent top-NNE shear sense, we do not consider this explanation likely. Furthermore, displacement-length scaling relationships for faults [53] indicate that the mapped trace length of a fault is approximately linearly proportional to the amount of displacement on that fault. Below we argue for a minimum displacement of ~50 km on the NPEFS on Naxos. According to the discussion by [53], such a displacement can only occur on faults that have considerable lateral extent exceeding by far the distance between Naxos and Paros. In summary, based on preliminary field work and geochronological data, we consider option (1) most likely. Although there are differences in the timing of fault slip on the NPEFS between Naxos and Paros, the slip rates as derived from the ZFT data are similar (Table 3). With decreasing temperature it seems that slip on the Naxos segment of the NPEFS in general increased whereas it remained fairly constant on the Paros segment.

Temporal variations of the slip rate

Excluding the problematic AHe ages, our data show that the slip rate for the brittle NPEFS exposed on Naxos is ~8-9 km Myr^{-1} over the temperature range from ~300°C to ~40°C. The slip rate estimated for the ductile NPEFS on Naxos is ~5-6 km Myr^{-1} [6] and thus smaller.

The slip rates calculated previously [6] and in this study assume that isotherms are unaffected by faulting. Therefore, at first glance the high slip rates at low temperatures might simply reflect advection and quenching of isotherms in the footwall slip direction of the NPEFS. Thermal modeling [48] showed that isotherms quickly approach a steady-state value within a few million years after the onset of extension. Our thermal modelling demonstrated that only the slip rate obtained from hornblende is significantly affected by thermal advection. For the lower temperature systems the amount of underestimation is insignificant. In the case of the NPEFS the intrusion of the Naxos granodiorite at ~12 Ma would have caused an additional thermal perturbation, which may have also affected the low-temperature radiometric systems. Again, our thermal modeling shows that slip rates are not significantly affected by the granodiorite intrusion. Furthermore, the similar cooling history and slip-rate evolution of the Carboniferous basement of Paros, the small S-type granites and the large Naxos granodiorite make it unlikely that the heat supplied by the granodiorite caused a significant thermal perturbation. We argue that cooling due to rapid slip on the NPEFS controlled footwall cooling.

What is the significance of the different slip rates reported by previous work [6] for the ductile NPEFS and those reported in this study for the brittle NPEFS on Naxos? Four explanations are considered, the first two of which argue for a constant slip rate whereas options (3) and (4) discuss an increase in the slip rate in the brittle crust: (1) The average ductile slip rate of ~5-6 km Myr^{-1} of John and Howard (1995) significantly underestimates the true slip rate due to pronounced advection of isotherms. According to our modeling the slip rate inferred from hornblende age data would underestimate the true rate by ~30%, suggesting a true slip rate of ~6.5 km Myr^{-1}. However, the problem is that we do not exactly know when ductile shearing commenced. In the modeling we assumed that slip started at peak temperature, which maximizes the possible effects of isotherm advection. Several authors [19, 31] have argued that shearing probably commenced before the peak of high-temperature metamorphism at 20-16 Ma. Therefore, the isotherms might have already achieved conditions close to steady state at ~16 Ma in which case the average slip rate estimated for the ductile part of the NPEFS [6] does not seriously underestimate the true slip rate.

(2) Due to the large errors obtained on the slip rates one could argue that the slip rate remained constant across the brittle/ductile transition. However, the MSWD values and the

probability of fit indicate that the calculated errors are overestimated, particularly for the FT data.

(3) Therefore, we believe that the data broadly suggest an acceleration of the slip rate in the later stages of faulting when the footwall reached the brittle crust and the fault zone narrowed considerably. The AFT data from Naxos support this option. If a slip rate was calculated from the early cooled samples Na3 through Na6, a rate of 6.5 (+15.7/-3.8) km Myr^{-1}, which is similar to the ZFT slip rate from Naxos and the AFT rate from Paros, would be obtained. If samples Na1 and Na2 are included in the AFT slip-rate calculation, the rate increases to 8.0 (+11.8/-3.0) km Myr^{-1}. Because Na1 and Na2 are the last to be exhumed, we envisage that this increase in the slip rate could reflect an increase in fault speed during the final stages of slip. Although the errors in both slip rate calculations are large, this interpretation is fully supported by the numerical modeling, which was also able to better replicate the particular age measurements with this scenario (see above).

The narrowing of the deforming zone indicates localization of deformation during decreasing temperatures as the NPEFS was exhumed. We argue that the intrusion of the huge arc-related granodiorite into the footwall directly beneath and within the NPEFS on Naxos, the widespread subsequent formation of frictional melts along the fault surface as documented by the numerous pseudotachylites and extensive fluid circulation along the fault surface might have been the most important factors for increasing the slip rate in the brittle crust. We suggest that the intrusion of the granodiorite increased the weakness considerably within the narrow deforming zone in the brittle crust and accelerated the slip rate as the footwall of the NPEFS was exhumed and cooled. The succeeding formation of pseudotachylite by frictional melting during seismogenic faulting documents transient single events of slip and the fact that there are numerous pseudotachylites in a swarm most probably resulted from prolonged seismogenic shear motion at the detachment. In fact, the AFT, ZHe and AHe ages overlap in time with the K/Ar pseudotachylite age [35] suggesting a causal relationship between pseudotachylite formation and acceleration of fault slip in the brittle regime. The important role of melt lubrication during deformation has been demonstrated by [54]. It was argued that weakening of the crust in the presence of melt leads to a drastic increase in deformation rates due to a pronounced drop in strength across zone occupied by melt [54]. We propose that this drop in strength would be even more pronounced in the brittle crust than in the ductile regime for which the melt weakening was originally proposed [54]. Furthermore, the fluids circulating along the fault surface were overpressurized and contributed to fault-zone weakening in the brittle crust on Naxos.

Extension of granitic crust has been analysed by [55] using a unified, fully coupled thermal-mechanical model in which brittle and ductile layers develop a natural transition as a function of the state variables (pressure, deviatoric stress, temperature, strain rate). This work shows that the main storage of elastic energy lies in the brittle/ductile transition zone, which is a zone of maximum energy dissipation and a local heat source (shear heating). The brittle/ductile transition is the focus of shear localization owing to the greatest weakening in relation to the thermal effects of shearing. It evolves through cascading instabilities with extreme weakening by nonlinear feedback of small-scale interacting faults coalescing to form an extremely weak detachment layer [55]. According to [56], upper crustal faulting is controlled by individual creep bursts resulting in earthquakes in the brittle fields. We argue that the pseudotachylite swarm in the Naxos granodiorite documents such earthquakes.

If indeed extension in the upper crust is faster than extension of the lower crust a space problem arises and a tear or gap should open in the lower crust at a rate of ~2-4 km Myr^{-1}. We consider it feasible that the increased rate of upper crustal extension triggered diffuse extension in the lower crust, i.e. the lower crust extended at the same rate but extension was not as localized as in the upper crust. Another possibility would be that lateral influx of ductile material or emplacement of melts filled the gap(s) in the lower crust. Underplating of mafic melts in the lower crust would in turn provide a possible explanation for the anomalously high Miocene temperatures and migmatization on Naxos in the Miocene.

However, note that the ductile slip rates represent the time span from ~16-12 Ma and the brittle rate from ~12-8 Ma, i.e. the different rates did not occur at the same time and record the temporal progression of the slip rate in the footwall. Therefore, explanation (4) considers that the increase in the slip rate does not necessarily imply faster extension of the upper crust but simply an increase in the rate of extension in the Aegean at ~12 Ma. At about ~12-10 Ma a number of new extensional detachments formed in the Aegean [11, 14, 56, 57] and this might imply a new extensional pulse.

Slip rate and minimum offset on the NPEFS

The data from [6] suggest a minimum average slip rate of ~5-6 km Myr^{-1} in the ductile NPEFS and our new data imply an average slip rate of ~8-9 km Myr^{-1} for the brittle NPEFS on Naxos. The slip rates and the timing of slip allow a minimum displacement calculation for the southern segment of NPEFS on Naxos. In the ductile regime between ~16-12 Ma a minimum offset of ~20 km results (note that if slip commenced >20 Ma offset would be >40 km) while in the brittle crust between ~12-8 Ma a minimum offset of ~32 km results, giving a

minimum total displacement of ~50 km on the NPEFS. The data suggest, if offset on the Ios detachment is also considered (Fig. 1) [56, 57], that the thin and non-metamorphosed Cycladic ophiolite nappe in the hangingwall of the Naxos/Paros extensional fault system is a far-travelled, dismembered extensional nappe that may have been derived from the Island of Crete. The long-lived activity and the high slip rate lends support to the hypothesis that much of the ~>250 km of post Oligocene extension in the Aegean Sea was resolved on a few major and fast slipping normal fault systems.

Conclusions

This study demonstrates the benefits of adopting a multi-thermochronometer approach to constrain the spatial and long-term evolution of an extensional fault system. Our new results seem to indicate that the slip rate on the NPEFS exposed on Naxos might increase from ~5-6 km Myr^{-1} to ~8-9 km Myr^{-1} across the brittle/ductile transition. Based on the available evidence we consider it most likely that the acceleration in slip rate was due to the intrusion of a large granodiorite body into the narrowing fault zone and subsequent pseudotachylite formation in the brittle crust. We propose that the brittle/ductile transition controlled the intrusion of the granodiorite and that melting might controlled an increase slip across the brittle/ductile transition.

Acknowledgements. Funded by the Deutsche Forschungsgemeinschaft (grants Ri 538/16, /18, /23 and Graduiertenkolleg 392). We are grateful to K.A. Farley and L. Hedges for assistance and forbearance during (U-Th)/He dating at California Institute of Technology Thanks to the Texas Advanced Computing Center which provided the computational resources necessary to accomplish the modeling. Careful reviews by R. Brady and J. Wijbrans helped to focus our ideas and to improve the paper.

References

[1] R.L. Armstrong, Low-Angle (Denudation) Faults, Hinterland of the Sevier Orogenic Belt, Eastern Nevada and Western Utah, Geol. Soc. Am. Bull. 83 (1972) 1729-1754.

[2] G.S. Lister, G. Banga, A. Feenstra, Metamorphic core complexes of Cordilleran type in the Cyclades, Aegean Sea, Greece, Geology 12 (1984) 21-25.

[3] G.S. Lister, G.A. Davis, The origin of metamorphic core complexes and detachment faults during Tertiary continental extension in the northern Colorado River region, USA, J. Struct. Geol. 11 (1989) 65-94.

[4] K.A. Howard, D.A. Foster, Thermal and unroofing history of a thick, tilted Basin-and-Range crustal section in the Tortilla Mountains, Arizona, J. Geophys. Res. 101 (1996) 511-522.

[5] D.A. Foster, A.J.W. Gleadow, S.J. Reynolds, P.G. Fitzgerald, The denudation of metamorphic core complexes and the reconstruction of the Transition Zone, west-central Arizona: constraints from apatite fission-track thermochronology, J. Geophys. Res. 98 (1993) 2167-2185.

[6] B.E. John, K.A. Howard, Rapid extension recorded by cooling-age patterns and brittle deformation, Naxos, Greece, J. Geophys. Res. 100 (1995) 9969-9979.

[7] D.A. Foster, B.E. John, Quantifying tectonic exhumation in an extensional orogen with thermochronology: examples from the southern Basin and Range province, in: U. Ring, M.T. Brandon, G.S. Lister, S.D. Willett (Ed.), Exhumation processes: Normal faulting, ductile flow and erosion, Geol. Soc. Special Publication London 154 (1999) 343-364.

[8] D. Sorel, A Pleistocene and still-active detachment fault and the origin of the Corinth-Patras rift, Greece, Geology 28 (2000) 83-86.

[9] R.J. Brady, Very high slip rates on continental extensional faults; new evidence from (U-Th)/He thermochronometry of the Buckskin Mountains, Arizona, Earth Planet. Sci. Lett. 197 (2002) 95-104.

[10] U. Ring, T. Reischmann, The weak and superfast Cretan detachment, Greece: Exhumation at subduction rates in extrusion wedges, J. Geol. Soc. London 159 (2002) 225-228.

[11] U. Ring, S.N. Thomson, M. Bröcker, Fast extension but little exhumation: the Vari detachment in the Cyclades, Greece, Geol. Mag. 140 (2003) 245-252.

[12] D. McKenzie, Active tectonics of the Alpine-Himalayan belt: the Aegean Sea and surrounding regions, Geophys. J. Roy. Astr. S. 55 (1978) 217-254.

[13] L.C. Vandenberg, G.S. Lister, Structural analysis of basement tectonites from the Aegean metamorphic core complex of Ios, Cyclades, Greece, J. Struct. Geol. 18 (1996) 1437-1454.

[14] C. Kumerics, U. Ring, S. Brichau, J. Glodny, J.-P. Monie, The extensional Ikaria shear zone and associated brittle detachments faults, Aegean Sea, Greece, J. Geol. Soc. London, 162, in press.

[15] U. Ring, P.W. Layer, T. Reischmann, Miocene high-pressure metamorphism in the Cyclades and Crete, Aegean Sea, Greece: Evidence for large-magnitude displacement on the Cretan detachment, Geology 29 (2001) 395-98.

[16] U. Ring, C. Johnson, R. Hetzel, K. Gessner, Tectonic denudation of a Late Cretaceous–Tertiary collisional belt: regionally symmetric cooling patterns and their relation to extensional faults in the Anatolide belt of western Turkey, Geol. Mag. 140 (2003) 421-441.

[17] S.N. Thomson, U. Ring, Thermochronologic evaluation of post-collision extension in the Anatolide Orogen, western Turkey, Tectonics (in press).

[18] D.L. Kohlstedt, B. Evans, S.J. Mackwell, Strength of the lithosphere: Constraints imposed by laboratory measurements, J. Geophys. Res. 100 (1995) 17587-17602.

[19] I.S. Buick, The late Alpine evolution of an extensional shear zone, Naxos, Greece, J. Geol. Soc. London 148 (1991) 93-103.

[20] P. Gautier, J.P. Brun, L. Jolivet, Structure and kinematics of upper Cenozoic extensional detachment on Naxos and Paros (Cyclades islands, Greece), Tectonics 12 (1993) 1180-1194.

[21] F. Henjes-Kunst, H. Kreuzer, Isotopic dating of pre-Alpidic rocks from the island of Ios (Cycladies, Greece), Contrib. Mineral. Petr. 80 (1982) 245-253.

[22] J. Lee, G.S. Lister, Late Miocene ductile extension and detachment faulting, Mykonos, Greece, Geology 20 (1992) 121-24.

[23] P. Gautier, J.P. Brun, Crustal-scale geometry and kinematics of late-orogenic extension in the central Aegean (Cyclades and Evvia), Tectonophysics 238 (1994) 399-424.

[24] R. Altherr, H. Kreuzer, I. Wendt, H. Lenz, G.H. Wagner, J. Keller, W. Harre, A. Höhndorf, A late Oligocene/early Miocene high temperature belt in the Attic-Cycladic crystalline complex (SE Pelagonian, Greece), Geol. Jahrb. E23 (1982) 97-164.

[25] J.R. Wijbrans, M. Schliestedt, D. York, Single grain argon laser probe dating of phengites from the blueschist to greenschist transition on Sifnos (Cyclades, Greece), Contrib. Mineral. Petr. 104 (1990) 582-593.

[26] F. Tomaschek, A. Kennedy, I.M. Villa, C. Ballhaus, Zircons from Syros, Cyclades, Greece - Recrystallization and mobilisation during high pressure metamorphism, J. Petrol. 44 (2003) 1977-2002.

[27] U. Ring, P.W. Layer, High-pressure metamorphism in the Aegean, eastern Mediterranean: Underplating and exhumation from the Late Cretaceous until the Miocene to Recent above the retreating Hellenic subduction zone, Tectonics 22 (2003), 1022, doi: 10.1029/2001ITC001350, 23p.

[28] M. Fytikas, F. Innocenti, P. Manetti, R. Mazzuoli, A. Peccerillo, L. Villari, Tertiary to Quaternary evolution of volcanism in the Aegean region, in: A.H.F. Robertson, J.E.

Dixon (Ed.), The geological evolution of the eastern Mediterranean, Geol. Soc. Special Publication London 17 (1984) 687-699.

[29] S. Keay, G. Lister, I. Buick, The timing of partial melting, Barrovian metamorphism and granite intrusion in the Naxos metamorphic core complex, Cyclades, Aegean Sea, Greece, Tectonophysics 342 (2001) 275-312.

[30] J.B.H. Jansen, R.D. Schuiling, Metamorphism on Naxos; petrology and geothermal gradients, Am. J. Sci. 276 (1976) 1225-1253.

[31] I.S. Buick, T.J.B. Holland, The P-T-t path associated with crustal extension, Naxos, Cyclades, Greece, in: J.S. Daly, R.A. Cliff, B.W.D. Yardley (Ed.), Evolution of Metamorphic Belts, Geol. Soc. Special Publication London 43 (1989) 365-369.

[32] E. Robert, Contribution à étude géologique des Cyclades (Grèce): l'île de Paros, Thèse de doctorat Paris-Sud (Orsay) (1982) 102 pp.

[33] J.R. Wijbrans, I. McDougall, Metamorphic evolution of the Attic Cycladic metamorphic belt on Naxos (Cyclades, Greece) utilizing $^{40}Ar/^{39}Ar$ age spectrum measurements, J. Metamorph. Geol. 6 (1988) 571-594.

[34] J.R. Wijbrans, I. McDougall, $^{40}Ar/^{39}Ar$ dating of white micas from an Alpine high-pressure metamorphic belt on Naxos (Greece): The resetting of the argon isotopic system, Contrib. Mineral. Petr. 93 (1986) 187-194.

[35] P.A.M. Andriessen, N.A.I.M. Boelrijk, E.H. Hebeda, E.H. Priem, T. Verdurmen, R.H. Verschure, Dating the events of metamorphism and granitic magmatism in the Alpine Orogen of Naxos (Cyclades, Greece), Contrib. Mineral. Petr. 69 (1979) 215-225.

[36] P.A.M. Andriessen, K-Ar and Rb-Sr age determinations on micas of impure marbles of Naxos, Greece: The influence of metamorphic fluids and lithology on the blocking temperature, Schweiz. Miner. Petrogr. Mitt. 71 (1991) 89-99.

[37] R.H. Sibson, Fault rocks and fault mechanisms, J. Geol. Soc. London 133 (1977) 191-213.

[38] T. Tagami, R.F. Galbraith, G.M. Yamada, G.M. Laslett, Revised annealing kinetics of Fission-tracks in zircon and geological implications, in: P. Van den Haute, F. De Corte, (Ed.), Advances in Fission-track Geochronology, Amsterdam, Kluwer Academic Press, (1998) 99-112.

[39] P.F. Green, I.R. Duddy, A.J.W. Gleadow, P.R. Tinegate, G.M. Laslett, Thermal annealing of fission tracks in apatite, 1.A qualitative description, Chem. Geol. 59 (1986) 237-253.

[40] P.W. Reiners, T.L. Spell, S. Nicolescu, K.A. Zanetti, Zircon (U-Th)/He thermochronometry: He diffusion and comparisons with $^{40}Ar/^{39}Ar$ dating, Geochim. Cosmochim. Acta 68 (2004) 1857-1887.

[41] T. Tagami, K.A. Farley, D.F. Stockli, Thermal sensitivities of zircon (U-Th)/He and fission-track systems, Abstracts of the Goldschmidt conference, Kyoto, Japan. Geochim. Cosmochim. Acta 68 (2003) p. 466.

[42] R.A. Wolf, K.A. Farley, D.M. Kass, Modelling of the temperature sensitivity of the apatite (U-Th)/He thermochronometer, Chem. Geol. 148 (1998) 105-114.

[43] A.J. Hurford, P.F. Green, The zeta age calibration of fission track dating, Chem. Geol. 1 (1983) 285-317.

[44] R.F. Galbraith, Statistical models for mixed ages, 7th Int. Workshop on Fission Track Thermochronology, Abstracts with Programs, Philadelphia, July 1992.

[45] M.A. House, B.P. Wernicke, K.A. Farley, T.A. Dumitru, Cenozoic thermal evolution of the central Sierra Nevada, California, from (U-Th)/He thermochronometry, Earth Planet. Sci. Lett. 151 (1997) 167-179.

[46] M.A. House, K.A. Farley, D. Stockli, Helium chronometry of apatite and titanite using Nd-YAG laser heating, Earth Planet. Sci. Lett. 183 (2000) 365-368.

[47] K.A. Farley, R.A. Wolf, L.T. Silver, The effect of long alpha-stopping distances on (U-Th)/He ages, Geochim. Cosmochim. Acta 60 (1996) 4223-4229.

[48] R.A. Ketcham, Thermal models of core-complex evolution in Arizona and New Guinea: Implications for ancient cooling paths and present-day heat flow, Tectonics 15 (1996) 933-51.

[49] C.R. Walcott, S.H. White, Constraints on the kinematics of post-orogenic extension imposed by stretching lineations in the Aegean region, Tectonophysics 298 (1998) 155-175.

[50] E. Hejl, H. Riedl, N. Soulakellis, P. van den Haute, H. Weingartner, Young Neogene tectonics and relief development on the Aegean islands of Naxos, Paros and Ios (Cyclades, Greece), Mitt. Österr. Geol. Ges., 93 (2003) 105-127.

[51] J.H. Rippon, Contoured patterns of the throw and hade normal faults in the Coal Measures (westphalian) of north-east Derbyshire, Proc. Yorks. Geol. Soc. 45 (1985) 147-161.

[52] D.C.P. Peacock, Displacements and segment linkage in strike-slip fault zones, J. Struct. Geol. 13 (1991) 1025-1035.

[53] P.A. Cowie, C.H. Scholz, Displacement-length scaling relationship for faults; data synthesis and discussion, J. Struct. Geol. 14 (1992) 1149-1156.

[54] L.S. Hollister, M.L. Crawford, Melt-enhanced deformation: A major tectonic process, Geology 14 (1986) 558-561.

[55] K. Regenauer-Lieb, D.A. Yuen, Positive feedback of interacting ductile faults from coupling of equation of state, rheology and thermal-mechanics: Physics of the Earth and Planetary Interiors, 142 (2004) 113–135, doi: 10.1016/j.pepi.2004.01.003.

[56] K. Regenauer-Lieb, B. Hobbs, A. Ord, On the thermodynamics of listric faults, Earth Planets Space, 56 (2004) 1111-1120.

[57] U. Ring, T. Brachert, C. Fassoulas, Middle Miocene graben development in Crete and its possible relation to large-scale detachment faults, Terra Nova 13 (2001) 297-304.

Figure captions

Figure 1. (a) Generalized tectonic map of Hellenides showing major tectonic zones, island of Naxos and major extensional fault systems, which represent latest generation of shallow-dipping, penetrative extensional structures. Also shown is the Mid Cyclades lineament [49]. Insert: Miocene to Recent thrust fronts in Mediterranean region and location of main map (modified from [11]). (b) Schematic NNE-SSW cross section showing nappe pile and major Miocene detachments in southern Aegean; Naxos/Paros extensional fault system (NPEFS) is syntectonic to arc-related Middle/Late Miocene granites (modified from [11]).

Figure 2. (a) Simplified geologic map of Naxos and Paros islands (isograds are from [30, 32], Mid Cyclades lineament from [49] and contact metamorphic aureole from [30]). (b) E-W cross section showing folding of NPEFS about N-S axes during top-NNE extension. (c) NNE-SSW cross section from Paros showing sample localities of thermochronologic samples relative to detachment fault. (d) NNE-SSW cross section of Naxos showing geochronologic samples relative to detachment fault. The figures are modified from [19, 20, 30]. Sample locations are indicated.

Figure 3. (a) Plot of zircon and apatite fission-track and (U-Th)/He ages (quoted at 2σ level) against distance in slip direction (also at 2σ level) for the brittle part of the NPEFS exposed on Naxos. Linear least squares regressions using Monte Carlo provides slip rates of 6.4 (+6.8/-2.2) km Myr^{-1} (ZFT), 13.2 (+9.4/-4.5) km Myr^{-1} (ZHe), 8.0 (+11.8/-3.0) km Myr^{-1} (AFT) and 9.1 (+5.3/-2.6) km Myr^{-1} (AHe). (b) Plot of zircon and apatite fission-track and zircon (U-

Th)/He ages (quoted at 2σ level) against distance in slip direction (also at 2σ level) for the brittle part of the NPEFS exposed on Paros. Slip rates are 6.9 (+11.4/-3.1) km Myr^{-1} (ZFT), 6.1 (+2.8/-1.6)km Myr^{-1} (ZHe) and 6.1 (+13.7/-3.5) km Myr^{-1} (AFT).

Figure 4. (a) Schematic composite NNE-SSW cross section showing the projection of sampling sites below NPEFS when dextral offset on Mid Cyclades lineament is restored. (b) Same cross section without Mid Cyclades lineament. Star marks position where break in ages occurs.

Table 1. Fission track data and sample information.
Table 2. (U-Th)/He data.
Table 3. Slip rates.

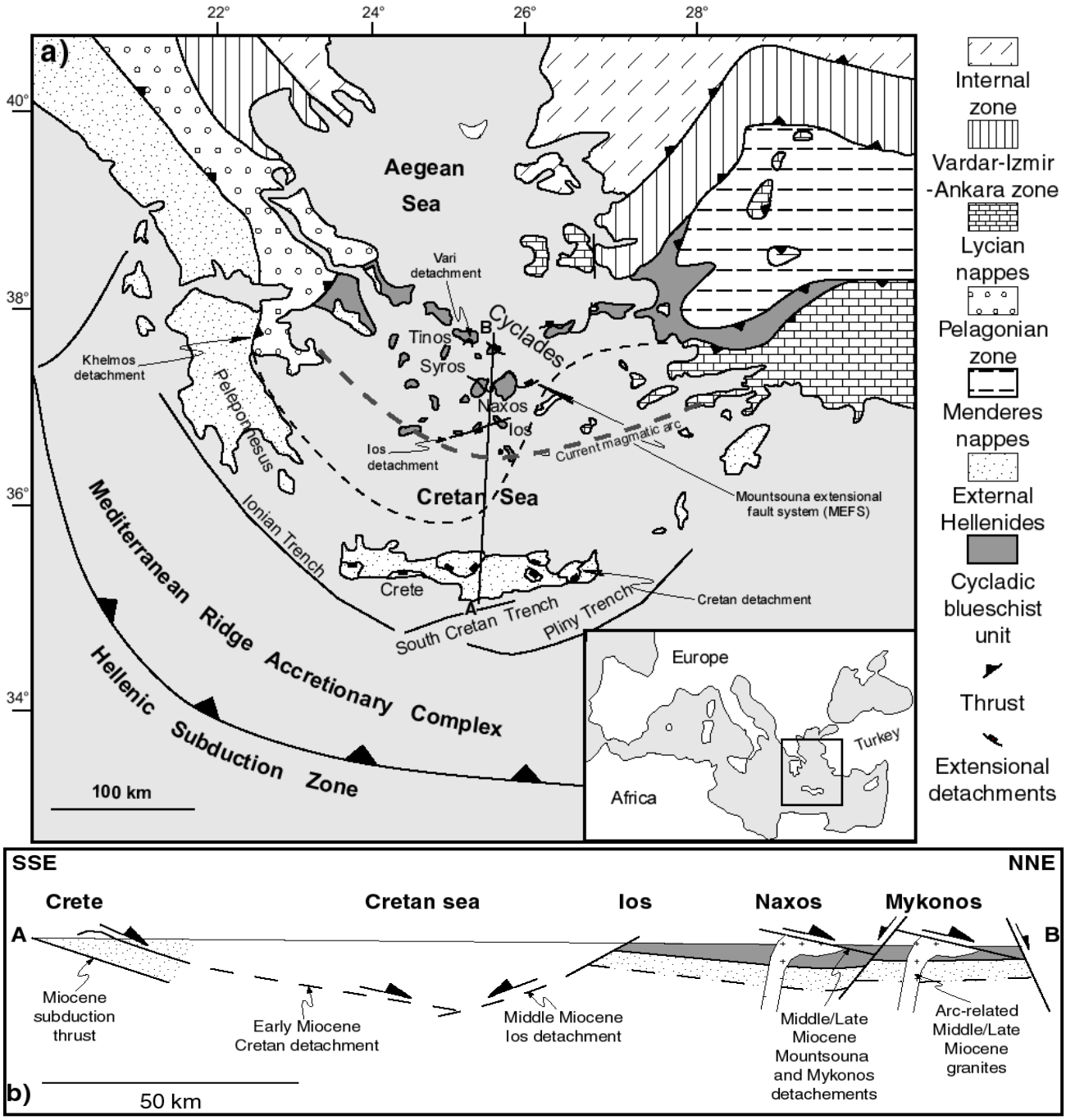

Fig. 1
Brichau et al.

Fig. 2
Brichau et al.

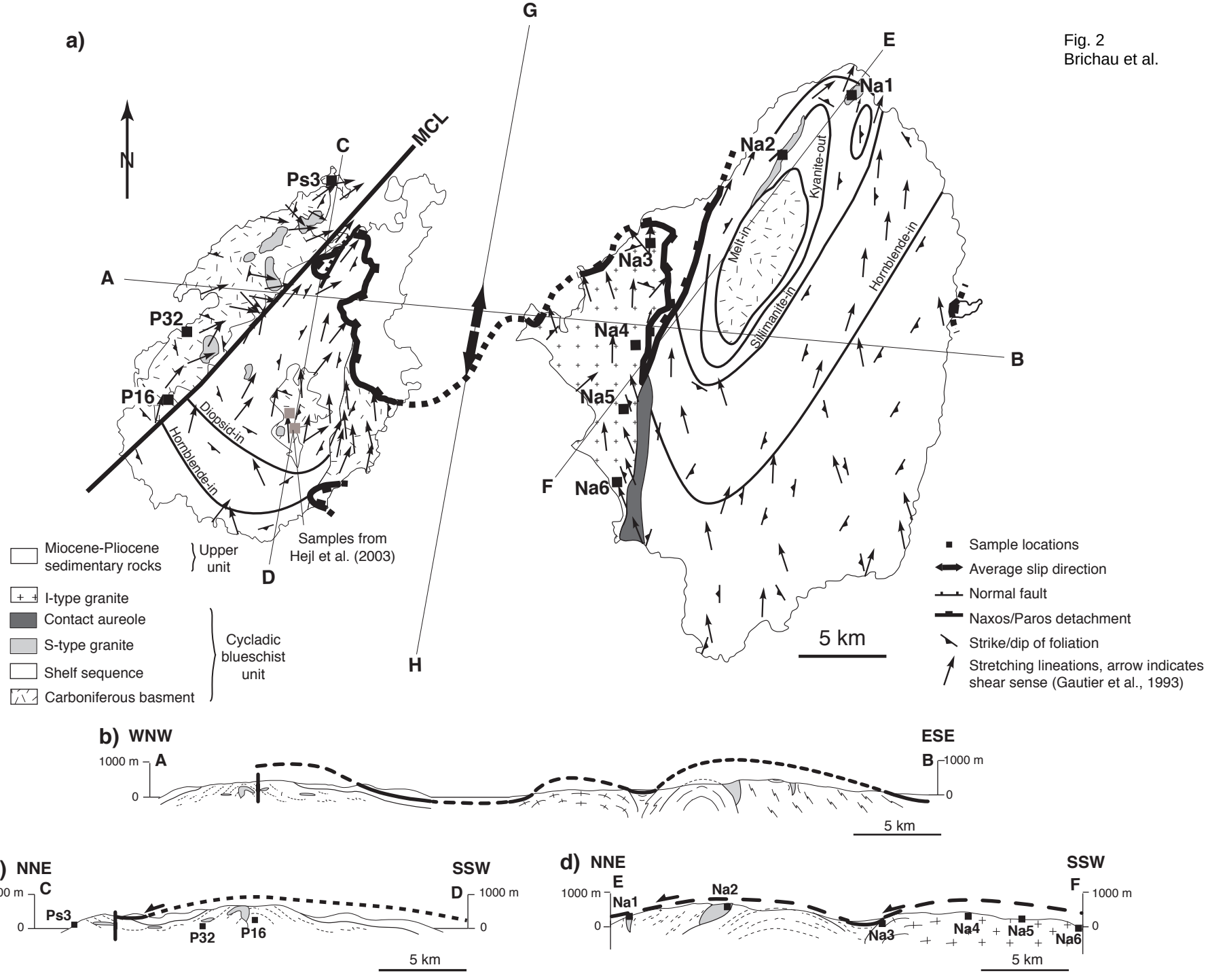

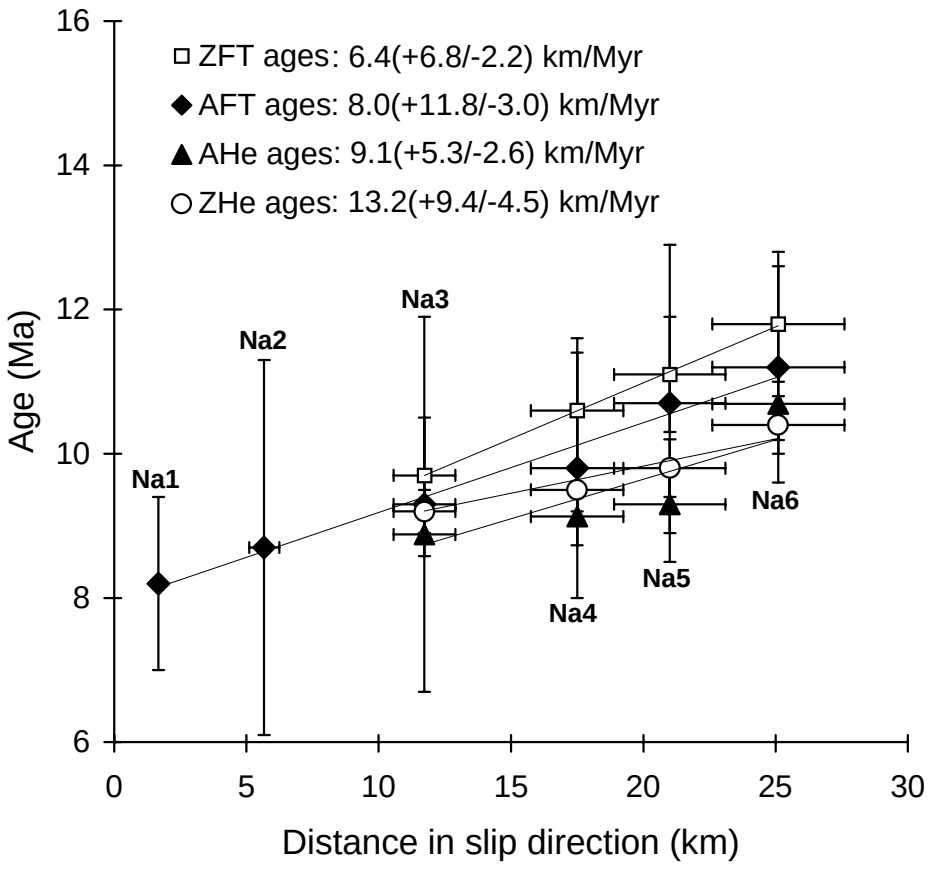

Fig 3a
Brichau et al.

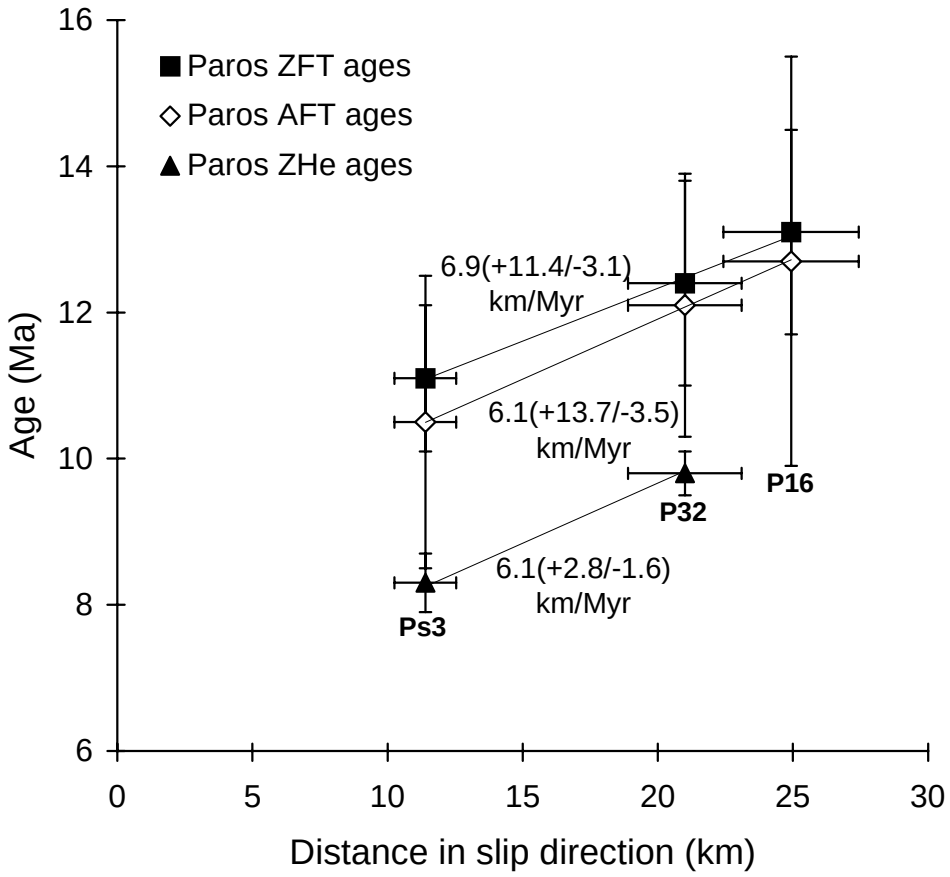

Fig 3b
Brichau et al.

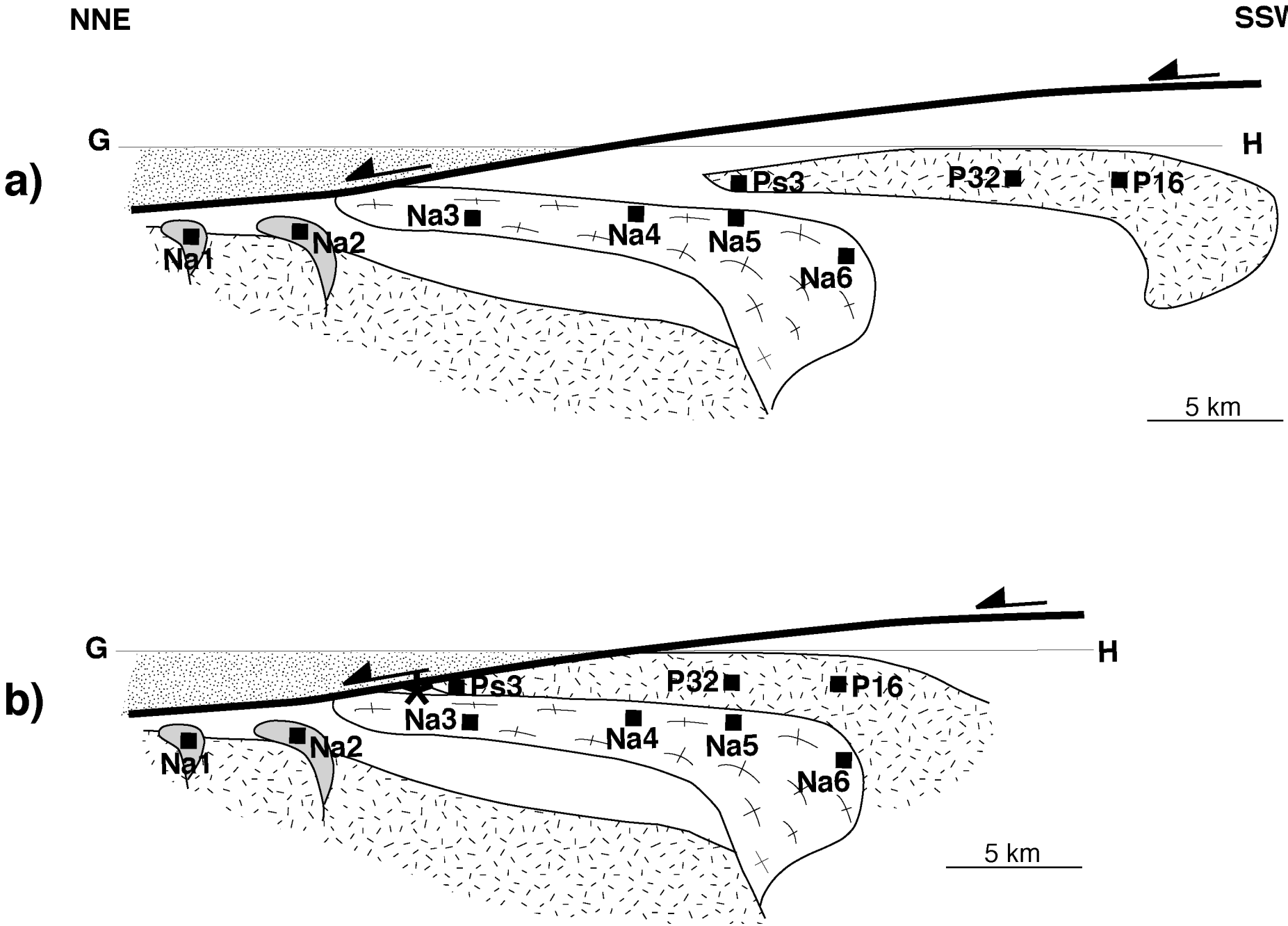

Fig. 5
Brichau et al.

Table 1. Fission track data and sample information

Sample no. (rock type)	Elevation (m)	Distance in slip direction (km)	Mineral	No. of crystals	Track density (x10^6 tr cm^{-2}) ρd (Nd)	ρi (Ni)	ρs (Ns)	Pχ2 (%)	U (ppm)	Mean FT age (Ma)	track length (μm)	StD (μm)	No. of tracks measured
NAXOS													
Na 1 (S-type granite)	30	1.7 ± 1	apatite	20	1.268 [15751]	0.168 [213]	4.313 [5482]	38.1	42.5	**8.2 ± 1.2**			
Na 2 (S-type granite)	175	5.7 ± 1	apatite	11	1.260 [15751]	0.062 [46]	1.497 [1112]	90.1	14.8	**8.7 ± 2.6**	14.5 ± 0.2	1.2	32
Na 3 (I-type granite)	70	11.7 ± 1	apatite	17	1.244 [15751]	0.160 [50]	3.562 [1115]	94.0	35.8	**9.3 ± 2.6**	14.7 ± 0.2	1.1	25
			zircon	14	0.321 [4089]	4.421 [1070]	9.343 [2261]	63.6	1068.1	**9.7 ± 0.8**			
Na 4 (I-type granite)	102	17.5 ± 1	apatite	20	1.236 [15751]	0.314 [132]	6.610 [2776]	96.9	66.8	**9.8 ± 1.8**			
			zircon	16	0.318 [4089]	3.883 [1262]	7.388 [2401]	99.4	853.8	**10.6 ± 0.8**			
Na 5 (I-type granite)	130	21.0 ± 1	apatite	17	1.204 [15751]	0.254 [108]	4.763 [2029]	67.7	49.4	**10.7 ± 2.2**	14.5 ± 0.2	1.1	36
			zircon	17	0.307 [4089]	3.814 [1644]	6.710 [2892]	99.8	801.7	**11.1 ± 0.8**			
Na 6 (I-type granite)	2	25.1 ± 1	apatite	24	1.188 [15751]	0.192 [189]	3.368 [3321]	73.4	35.4	**11.2 ± 1.6**			
			zircon	14	0.304 [4089]	4.360 [1696]	7.118 [2769]	54.2	860.2	**11.8 ± 0.8**			
PAROS													
Ps3 (gneiss)	10	11.4 ± 1	apatite	17	1.288 [12069]	1.349 [126]	2.734 [2554]	83.6	26.5	**10.5 ± 2.0**	14.4 ± 0.2	0.8	29
			zircon	11	0.388 [4920]	30.96 [932]	6.904 [2078]	99.7	653.0	**11.1 ± 1.0**			
P32 (gneiss)	8	21 ± 1	apatite	19	1.272 [12069]	1.201 [196]	2.09 [3411]	97.9	20.5	**12.1 ± 1.8**	15.0 ± 0.2	1.0	33
			zircon	8	0.358 [4920]	23.11 [513]	4.234 [940]	95.3	434.4	**12.4 ± 1.4**			
P16 (gneiss)	15	24.9 ± 1	apatite	17	1.890 [18667]	0.69 [84]	1.709 [2080]	100	11.3	**12.7 ± 2.8**	14.7 ± 0.1	1.0	68
			zircon	7	0.374 [4920]	33.02 [591]	5.994 [1073]	100	588.2	**13.1 ± 1.4**			

Zircon and apatite fission-track ages were calculated using zeta factors of 127 ± 4 and 330 ± 8.5 determined by multiple analyses of standards following recommendations of [42]; central ages are reported; data are quoted to 2◊ level. Distance in fault slip direction for each individual sample has been measured from the north end of the Naxos island. Although absolute geographic sample location errors are ±5 m, we adopted conservative distance uncertainties of 1km (2σ) to encompass errors in determination of map distance in the slip direction, distance below the detachment surface, and lack of knowledge about possible intervening structures and the changes in relative sample positions during the transition across the "rolling hinge" from dipping along the detachment at depth to being at roughly equivalent elevation today.

Table 2. (U-Th)/He data

Sample no. (rock type)	Mineral	Number of grain analysed	He (nmol/g)	U (ppm)	Th (ppm)	F_T	He age (Ma)
NAXOS							
Na 3	Apatite	4	1.236	29.967	38.502	0.66	8.9 ± 0.5
(I-type granite)	Apatite	4	1.032	24.074	28.527	0.70	8.8 ± 0.5
	Apatite	4	1.171	28.301	38.297	0.64	9.0 ± 0.5
Mean			***1.146***	***27.447***	***35.109***	***0.67***	***8.9 ± 0.3***
	Zircon	1	19.335	469.4	79.2	0.79	9.2 ± 0.6
	Zircon	1	11.550	315.3	91.0	0.71	8.8 ± 0.5
	Zircon	1	24.330	559.1	237.5	0.76	9.6 ± 0.6
Mean			***18.405***	***447.9***	***135.9***	***0.75***	***9.2 ± 0.3***
Na 4	Apatite	4	1.971	39.365	73.202	0.70	9.1 ± 0.5
(I-type granite)	Apatite	4	2.831	57.980	113.118	0.67	9.1 ± 0.5
Mean			***2.401***	***48.672***	***93.16***	***0.69***	***9.1 ± 0.4***
	Zircon	1	37.728	1041.80	169.0	0.69	9.3 ± 0.6
	Zircon	1	63.701	1622.70	409.3	0.67	10.2 ± 0.6
	Zircon	1	45.313	1194.50	217.5	0.74	9.1 ± 0.5
Mean			***48.914***	***1286.333***	***265.267***	***0.70***	***9.5 ± 0.3***
Na 5	Apatite	4	1.634	36.265	50.561	0.69	9.1 ± 0.5
(I-type granite)	Apatite	4	1.866	38.457	58.350	0.70	9.4 ± 0.6
Mean			***1.750***	***37.361***	***54.456***	***0.70***	***9.3 ± 0.4***
	Zircon	1	22.375	544.9	87.8	0.75	9.7 ± 0.6
	Zircon	1	14.813	298.7	129.5	0.78	10.7 ± 0.6
	Zircon	1	10.580	244.4	59.6	0.78	9.7 ± 0.6
	Zircon	1	17.482	484.3	63.3	0.73	8.9 ± 0.5
Mean			***16.313***	***393.1***	***85.1***	***0.76***	***9.8 ± 0.4***
Na 6	Apatite	4	2.225	42.055	56.805	0.71	10.4 ± 0.6
(I-type granite)	Apatite	4	1.745	32.796	44.735	0.67	11.0 ± 0.7
Mean			***1.985***	***37.426***	***50.77***	***0.71***	***10.7 ± 0.5***
	Zircon	1	14.554	339.9	49.4	0.75	10.1 ± 0.6
	Zircon	1	28.304	691.9	111.3	0.68	10.6 ± 0.6
Mean			***21.429***	***515.9***	***80.4***	***0.72***	***10.4 ± 0.4***
PAROS							
Ps3	Zircon	1	4.813	138.6	43.4	0.73	8.1 ± 0.5
(gneiss)	Zircon	1	7.277	197.1	77.7	0.74	8.4 ± 0.5
Mean			***6.045***	***167.85***	***60.55***	***0.735***	***8.3 ± 0.4***
P32	Zircon	1	26.058	614.1	103.9	0.76	10.1 ± 0.6
(gneiss)	Zircon	1	15.335	352.1	72.0	0.75	10.1 ± 0.6
	Zircon	1	15.924	387.0	68.4	0.78	9.3 ± 0.6
Mean			***19.106***	***451.073***	***81.449***	***0.76***	***9.8 ± 0.3***

(U-Th)/He ages were performed by Nd:YAG laser heating for He extraction and ICP-MS for U-Th determinations at the University of Kansas for zircon and Caltech for apatite. The estimated analytical uncertainty for He ages is about 6% (2σ).

Table 3. Slip rates

Island	Method	Samples	Slip rate	Error +	Error -	χ^2	χ^2 red.	Prob. of fit
Naxos	Hbl Ar/Ar	-	**4.7***	3.5*	1.4*	-	-	-
Naxos	Biot K/Ar	-	**5.1***	0.6*	0.5*	-	-	-
Naxos	ZFT	Na3-Na6	**6.4**	6.8	2.2	0.013	0.006	0.995
Naxos	ZHe	Na3-Na6	**13.2**	9.4	4.5	2.108	1.054	0.523
Naxos	AFT	Na1-Na6	**8.0**	11.8	3.0	0.784	0.046	0.996
Naxos	AFT	Na3-Na6	**6.5**	15.7	3.8	0.093	0.047	0.955
Naxos	AHe	Na3-Na6	**9.1**	5.3	2.6	13.579	6.789	0.005
Paros	ZFT	Ps3, P32, P16	**6.9**	11.4	3.1	0.020	0.020	0.892
Paros	ZHe	Ps3, P32	**6.1**	2.8	1.6	-	-	1
Paros	AFT	Ps3, P32, P16	**6.1**	13.7	3.5	0.001	0.001	0.977

** Data from [6]. Hbl Ar/Ar= Hornblende Ar/Ar; Biot K-Ar= Biotite K-Ar; ZFT= Zircon Fission Track; ZHe= Zircon (U-Th)/He; AFT= Apatite Fission Track; AHe= Apatite (U-Th)/He.